Journal of the European Ceramic Society **15** (1995) 717–727

0955-2219/95/$9.50

0955-2219(95)00029-1

Polymer-Derived Si-Based Bulk Ceramics, Part II: Microstructural Characterisation by Electron Spectroscopic Imaging

Joachim Mayer,[a] D. Vinga Szabó,[a]* Manfred Rühle,[a] Martin Seher[b,c] & Ralf Riedel[d]

[a]Institut für Werkstoffwissenschaft, Max-Planck-Institut für Metallforschung, Seestr. 92, D-70174 Stuttgart, Germany
[b]Institut für Anorganische Chemie, Universität Stuttgart, Pfaffenwaldring 55, D-70550 Stuttgart, Germany
[c]Pulvermetallurgisches Laboratorium, Institut für Werkstoffwissenschaft, Max-Planck-Institut für Metallforschung, Heisenbergstr. 5, D-70569 Stuttgart, Germany
[d]Fachgebiet Disperse Feststoffe, Fachbereich Materialwissenschaft, Technische Hochschule Darmstadt, Hilpertstr. 31, D-64295 Darmstadt, Germany

(Received 2 August 1994; revised version received 7 February 1995; accepted 14 February 1995)

Abstract

The microstructure of polymer-derived Si-based ceramic materials was characterised with elemental distribution images produced by electron spectroscopic imaging. Depending on the processing conditions, a variety of different microstructures were obtained from the same precursor: without sintering additives, amorphous silicon carbonitride which is stable against crystallisation up to 1400°C is formed. In the presence of Al_2O_3 and Y_2O_3 as sintering additives, Si_3N_4/SiC-composite materials and Si_2N_2O ceramics are produced. Sintering a mixture of Si_3N4 powder with additional polysilane leads to a Si_3N_4/SiC-composite comprising nano-sized SiC inclusions in the Si_3N_4 grains. The development of the microstructure of the Si_3N_4/SiC composite materials was investigated as a function of the sintering temperature and of the concentration of the sintering additives. The observed microstructural changes lead to conclusions on the processes which occur during the sintering of the materials.

1 Introduction

A primary aim in the development of structural ceramics is to obtain control over both the mechanical properties and the macroscopic shape of the ceramic component. The mechanical properties of any material are governed by the microstructure. It is thus desirable to be capable of influencing the microstructure, via the starting material and the processing conditions, and to 'know' the result, via an efficient characterisation technique. In Part I[1] of our studies we have shown that preparing ceramic materials from polymer precursors potentially offers control of both the shape of the final ceramic product and of a variety of microstructural parameters, ranging from the synthesis of monolithic ceramics at low temperatures to the design of composite microstructures with several different phases.

In this paper we report on the results of our microstructural investigations on the polymer derived ceramic materials. In a systematic way we aim to gain insight into the relationships between microstructure and processing parameters. For characterisation, a new technique in transmission electron microscopy was used: electron spectroscopic imaging, (ESI).[2] With ESI, images showing the distribution of various elements in large specimen areas (several μm^2) at high resolution (2–3 nm) can be produced within short times (less than 1 min for one element). ESI is based on the use of an imaging energy filter and makes it possible to image the distribution of a certain element via the characteristic energy losses which an electron beam may suffer in inelastic scattering processes with the atoms in the sample. Hence, Energy Filtering Transmission Electron Microscopy (EFTEM) has become an important tool for the microstructural characterisation of composite microstructures.

In the last ten years considerable research has been devoted to the evaluation of microstructures in Si_3N_4 and SiC ceramics. For the sintering of Si_3N_4 ceramics, Al_2O_3 and Y_2O_3 are used as sintering additives in most cases. Sintering occurs via a liquid phase mechanism in which the solution of α-Si_3N_4 and reprecipitation of β-Si_3N_4 play an important role. Systematic studies with various

*Present address: Kernforschungszentrum Karlsruhe, IMF 3, Postfach 3640, D-76201 Karlsruhe, Germany.

amounts of sintering additive were carried out by Hayashi *et al.*[3] They found that diffusion through the liquid phase is the rate-limiting step in the growth of the Si_3N_4 crystals. Boberski *et al.*[4] investigated the intermediate sintering stages by quenching samples during the sintering process and found that the major densification step is correlated with the melting of the sintering additives at 1389°C and the $\alpha \rightarrow \beta$ transition occurring at 1615°C. Sintering of SiC with Al_2O_3 and Y_2O_3 as sintering additives has first been reported by Omori and Takei.[5] In a systematic TEM study, Kleebe[6] compared SiC and Si_3N_4 ceramics sintered with Al_2O_3 and Y_2O_3 and found that, in contrast to Si_3N_4, the SiC grains are not wetted by the liquid phase formed by the sintering additives. The microstructure of Si_3N_4/SiC-composite materials was investigated by several different groups.[7-11] The densification which can be obtained is significantly influenced by the amount of SiC added.[8] Higher contents of SiC particles inhibit complete densification and a number of pores remain in the final material. Indications for solution and reprecipitation of the SiC particles could only be found at temperatures above 1700°C. Under special conditions, inclusion of the SiC particles in the Si_3N_4 grains could be observed[9-11] which leads to an improvement of the mechanical properties. In the present paper we report on the sintering mechanisms observed in the Si_3N_4/SiC-composite materials prepared from polymer precursors. The temperature dependence of the sintering processes was studied by varying the maximum temperature. The dependence of the microstructure on the concentration of sintering additives was investigated by varying the amount of Al_2O_3 and Y_2O_3 which was added.

2 Experimental

2.1 Energy filtering TEM

In analytical electron microscopy the two methods mainly used, electron energy loss spectroscopy (EELS) and energy dispersive X-ray analysis (EDX), are based on focusing the probe on a small area of interest. The spectroscopic data are then analysed for each probe position. Two-dimensional chemical information can only be obtained by stepping the probe across the sample. For the light elements, EELS analysis is preferable because it offers a much higher detection efficiency. In principle, any EELS spectrometer can be treated as being part of the electron optical system of a TEM with the important property that the information on the image or diffraction pattern of the illuminated sample area is not completely lost but only heavily distorted while the electrons pass through the spectrometer. Within the past ten years, successful attempts have been made to correct these distortions electron-optically. One possibility is to combine four magnetic prisms in an Omega-like geometry where most of the electron optical aberrations are corrected by symmetry.[12] A different approach is to correct the distortions caused by one sector-magnet with an appropriate number of quadrupole and sextupole corrector elements.[13]

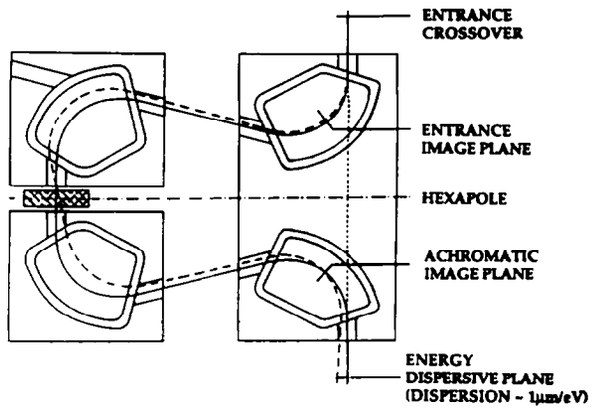

Fig. 1. Schematic drawing of the Omega filter. Through the symmetrical arrangement of magnetic prisms an image is transferred from the entrance image plane to the achromatic image plane. An energy loss spectrum of the illuminated sample area is formed in the energy dispersive plane.

In the present studies we have used a Zeiss EM 912 Omega which is the first commercially available EFTEM with an imaging Omega filter.[14] The design of the Omega filter is schematically shown in Fig. 1. An imaging filter combines two properties: (1) The symmetrical arrangement of prisms transfers an image without distortions to the achromatic image plane. (2) The energy dispersion of the whole arrangement of prisms causes the paths of electrons with different energies to separate and to form an energy loss spectrum at the exit surface of the Omega filter. In this energy dispersive plane, electrons within a defined energy loss interval $\Delta E_1 < \Delta E < \Delta E_2$ can be selected by inserting an energy selecting slit. Only these electrons will contribute to a magnified 'ESI' image which can be produced by focusing the following lenses of the projector system to the achromatic image plane.

2.2 Electron Spectroscopic Imaging (ESI)

Inner-shell excitation of the atoms by the beam electrons leads to characteristic edges in the energy-loss spectrum (Fig. 2). For energy losses above 100 eV the edges are located on top of a nearly exponentially decreasing background and the onset energies of each edge can be used to identify the individual chemical elements. The concentration of an element can be determined from an EELS spectrum if the pre-edge background is extrapolated and subtracted from the signal

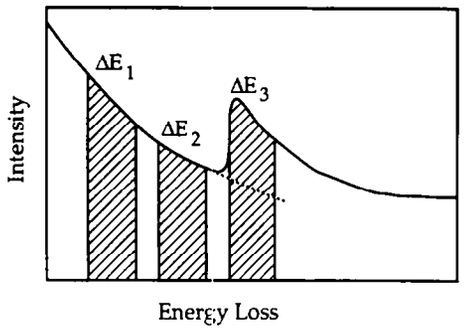

Fig. 2. Illustration of the three-window technique used to produce elemental distribution images. With the two ESI images acquired in front of the edge, an extrapolated background can be calculated and subtracted from the third image containing the element specific signal.

obtained above the edge. In ESI images this has to be done for each individual pixel. The easiest method for background subtraction, the three window technique, is illustrated in Fig. 2. Two ESI images are acquired in the background region before the edge and the extrapolated background is then subtracted from the ESI image containing the signal above the edge. As a result the difference image only contains intensity in the areas where the corresponding element is present in the sample and thus maps the distribution of this element. In the three window technique, however, the intensity in the difference image is not only depending on the concentration of the element but may also vary with thickness or the Bragg orientation of crystalline grains. Owing to the low intensity of the individual ESI images (up to a factor of 100–1000 less than the corresponding bright field image) the difference image will also contain considerable noise which makes it impossible to detect elements in very small concentrations (below 1 at%). The noise in the elemental distribution images can be reduced by special image processing techniques, which may result in a loss of resolution. The detection limits in elemental distribution images are as low as 1–2 monolayers, e.g. for segregants at grain boundaries.[15] The resolution limits are in the order of 2–5 nm, depending on the element and its concentration.

In the three window technique, the optimum position of the energy windows and their width depends on several parameters: (1) the intensity in the energy loss spectrum which decreases strongly with increasing energy loss; (2) the shape of the edge which only shows a sharp onset for the light elements, and (3) the width of the unstructured background region before the edge. The width and positions of the windows which we have used have been determined in an empirical way and are listed in Table 1. In the case of the Si–K edge at 1836 eV the slope of the decreasing background is so small that it can be extrapolated by a horizontal line. In this case, only one background image has to be acquired which is then simply subtracted from the image containing the signal.

Table 1. List of elements investigated by ESI. The energy losses of the edges, ΔE, and the centre of the windows, $\Delta E_1 ... \Delta E_3$, are given in eV.

Element	*Edge*	ΔE	ΔE_1	ΔE_2	ΔE_3	*Window width* ∂E
C	K	284	255	275	295	15
N	K	401	370	390	410	15
O	K	532	500	520	540	15
Si	K	1836	1740	1810	1880	50
Si	K	1836	—	1800	1880	50
Si	L	199	180	194	208	10

In most of the cases, the distribution of several elements will be studied in one sample area. The resulting elemental distribution images can be combined in one image by using different colours for each element and overlaying the individual images. If two or more of the elements under investigation are present in one sample area mixed colours will occur. Mixed colours thus reveal important information on the occurrence of phases which contain more than one of the elements under investigation.

2.3 High-resolution TEM

For some of the materials analysed, high-resolution TEM has been employed in order to distinguish between structurally amorphous and microcrystalline material. These studies were performed on a Jeol 4000 EX operated at 400 kV.

2.4 TEM specimen preparation

The samples sintered at lower temperatures or at a lower concentration of the sintering additives exhibit extremely high brittleness and thus low mechanical stability. Self-supporting TEM specimens could not be made out of these brittle samples and a special technique had to be applied. The method is based on the use of special cylindrical holders which are made out of alumina. The holders contain a slit into which a thin slice of the material (200–300 μm thick) is glued which gives the necessary mechanical support to the brittle material. Subsequently the holders are sectioned into thin discs from which TEM samples are made in the conventional way by polishing, dimpling and ion milling. Details of the technique were published elsewhere.[16]

3 Results and Discussion

As described in Part I of this work,[1] the Si-based materials produced by pyrolysis of Si-containing

Table 2. Empirical formulae of the polymeric precursors used and molar ratio of the final ceramic products (for details see Part I[1])

Empirical formulae†	*Abbreviation*	*Final ceramic material*††
$[-CH_3SiH-NH-]_m[-(CH_3)_2Si-NH-]_n$	PHMSN	$Si_{1.7}C_{1.0}N_{1.6}$
$[-CH_3SiH-N=]_m[-CH_3SiCl-N=]_n$	PCMSN	$Si_{1.7}C_{1.0}N_{1.5}$
$[[(CH_3)_2Si]_5[CH_3Si(C_6H_5]]_n$	PMPS	$SiC_{2.0}$

†Simplified formulae derived from analytical measurements.
††Composition obtained after pyrolysis of the precursor at 1000°C under Ar atmosphere.

polymer precursors can be classified according to the resulting microstructure. Monolithic silicon carbonitrides which consist entirely of an amorphous phase can be produced directly by pyrolysis of the compacted polymer. Dense ceramic composites formed by the crystalline phases Si_3N_4, Si_3N_4 containing SiC, or Si_2N_2O can be produced by adding sintering additives prior to pyrolysis. Both the chemistry of the metal–organic precursors and of the oxidic sintering additives can be varied in wide ranges with resultant changes in the microstructure. For the different precursors the following abbreviations will be used: poly(hydridomethyl)-silazane = PHMSN, poly(chlorhydridomethyl)silazane = PCMSN, poly(methylphenyl)silane = PMPS. The chemical formulae of the polymers have been derived from analytical investigations and are summarised in Table 2. A mixture of Al_2O_3 and Y_2O_3 in various amounts has been used as sintering additives in all cases.

3.1 PHMSN-derived monolithic Silicon Carbonitride

The monolithic silicon carbonitride was prepared by pyrolysis of the shaped infusible polysilazane precursor (PHMSN) at 1000°C under argon. Details of the preparation and characterisation of the material in terms of density and porosity are described in Part I. The TEM investigations showed that the sample material contains pores with diameters between 100 and 1000 nm. By SEM the existence of some larger pores with diameters of up to 10 μm could be seen. By electron diffraction in the TEM it could be verified that the samples are completely amorphous. The analysis of EELS spectra confirmed the presence of Si, N and C in the amorphous ceramic material while oxygen was below the detectivity limit (< 1 at%).

In Fig. 3, a TEM bright field image of the amorphous silicon carbonitride is compared with the ESI images obtained for C and N. The intensity variation in both ESI images is caused by the thickness changes visible in Fig. 3(a). In very thin areas of the specimen, e.g. close to the edge of the sample, the ESI image intensity is low due to the small number of atoms present. For increasing thickness, but below the mean free path for inelastic scattering, the intensity in the ESI images increases. Finally, for thicknesses above 20–30 nm, the intensity decreases again due to the occurrence of multiple inelastic scattering, which increases the background but decreases the intensity gain at the onset energy of an edge in the energy loss spectrum. However, in Figs 3(b) and (c) the same intensity ratio is always obtained for areas of constant thickness. Thus, the distribution of C and N in the amorphous material is homogeneous down to the resolution limit of about 2 nm. No indication for the precipitation or nucleation of Si_3N_4, SiC or pure carbon and elemental silicon was found. According to these electron microscopic findings, the polysilazane-derived silicon carbonitride can be described as a silicon-based amorphous ceramic containing $SiN_{4-x}C_x$ units with $0 < x < 4$.

Finally, quantitative elemental analytical investigations (for experimental details see Part I,[1]) yielded molar ratios which can be represented by the empirical formula $Si_{1.8}N_{1.6}C_{1.0}$ for the PHMSN

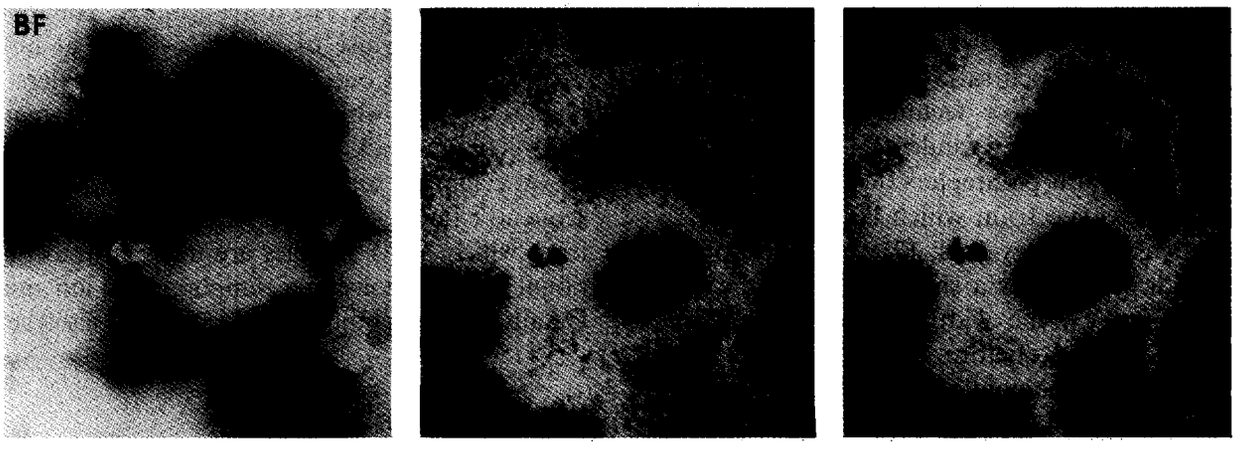

Fig. 3. Monolithic silicon carbonitride after pyrolysis at 1000°C. Comparison between bright field image and the elemental distribution images obtained for carbon and nitrogen. The thickness dependent intensity variation is the same in both distribution images confirming that C and N are distributed homogeneously in the material.

derived silicon carbonitride. Pyrolysis of PCMSN under the same conditions results in a silicon carbonitride with the composition $Si_{1.7}N_{1.5}C_{1.0}$.

3.2 PCMSN-derived Si_3N_4/SiC-composite

Polycrystalline Si_3N_4/SiC composites were produced by sintering of the amorphous PCMSN derived silicon carbonitride at different temperatures under nitrogen atmosphere. Various amounts of Y_2O_3 and Al_2O_3 were added as sintering additives prior to pyrolysis. Details of the processing conditions are described in Part I.[1]

In order to obtain insight into the formation of the microstructure during the sintering process, two series of experiments were carried out. The evolution of the microstructure with increasing sintering temperature and constant additive content was studied at four different temperatures between 1400°C and 1850°C. The dependence of the resulting microstructure on the concentration of the sintering additives at constant sintering temperature was investigated by varying the amount of sintering additives between 5 and 15 wt%. In the following, the microstructure obtained after heat treatment at the highest sintering temperature (1850°C) will be discussed first in order to facilitate comparison with the results obtained in the intermediate stages.

3.2.1 Microstructure after sintering at 1850°C

By sintering the material with 15 wt% sintering additives at 1850°C for 1 h, a ceramic composite with high density and low porosity is obtained. In Fig. 4, a bright field image of a thin area of the TEM specimen is shown. The microstructure consists of crystalline particles with grain sizes ranging from 50 nm to 1 μm and an oxidic glassy phase. The phase composition is revealed by the ESI image in Fig. 4(b). The elemental distribution of C, N and O is imaged in red, green and blue colour, respectively. The corresponding phases are SiC, Si_3N_4 and the amorphous oxide, which can thus clearly be identified. The average size of the SiC grains is generally smaller and less uniform than the size of the Si_3N_4 grains. The ESI images show that there is a tendency of the SiC grains to form clusters. In the material with 15% sintering additives, the Si_3N_4 grains and the individual or clustered SiC grains are separated by extended areas containing the amorphous oxide. X-ray investigations revealed that both crystalline phases are formed in the β-modification, i.e. the materials consist of β-Si_3N_4 and β-SiC.

3.2.2 Evolution of microstructure with temperature

By X-ray diffraction of the heat treated materials (see Part I[1]) it could be shown that, at temperatures below 1400°C, no changes in the phase composition occur and that the amorphous phase produced by the pyrolysis at 1000°C does not start to crystallise nor to react with the sintering additives. At temperatures around 1400°C, however, a rapid onset of crystallisation could be detected. This is presumably caused by the formation of a liquid phase by melting of the sintering additives.

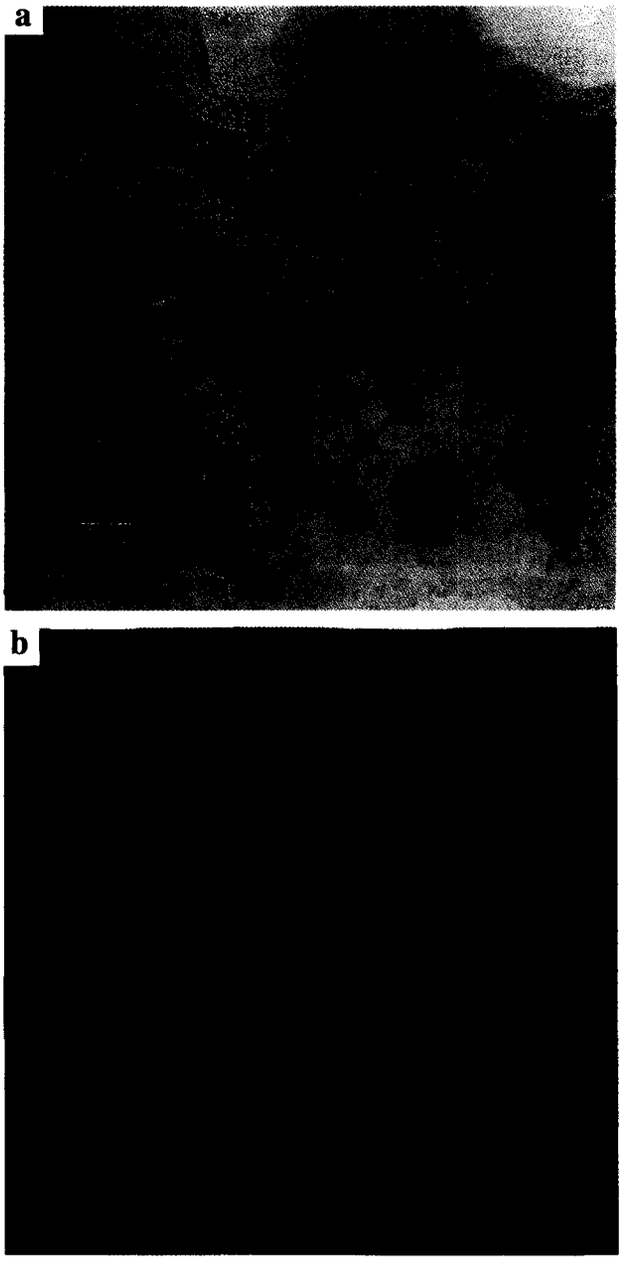

Fig. 4. Si_3N_4/SiC-composite material after sintering for 1 h at 1850°C. (a) Bright field image showing the microstructure; (b) Combined elemental distribution image for carbon (red), nitrogen (green) and oxygen (blue), showing the distribution of the SiC, Si_3N_4 and the amorphous oxide, respectively.

The microstructure which was obtained after a heat treatment of 1 h at 1400°C is shown in Fig. 5 (a). Irregularly shaped grains with dimensions between 50 and 300 nm can be observed. The grains are embedded in a matrix formed by a glassy phase. These areas can clearly be distinguished

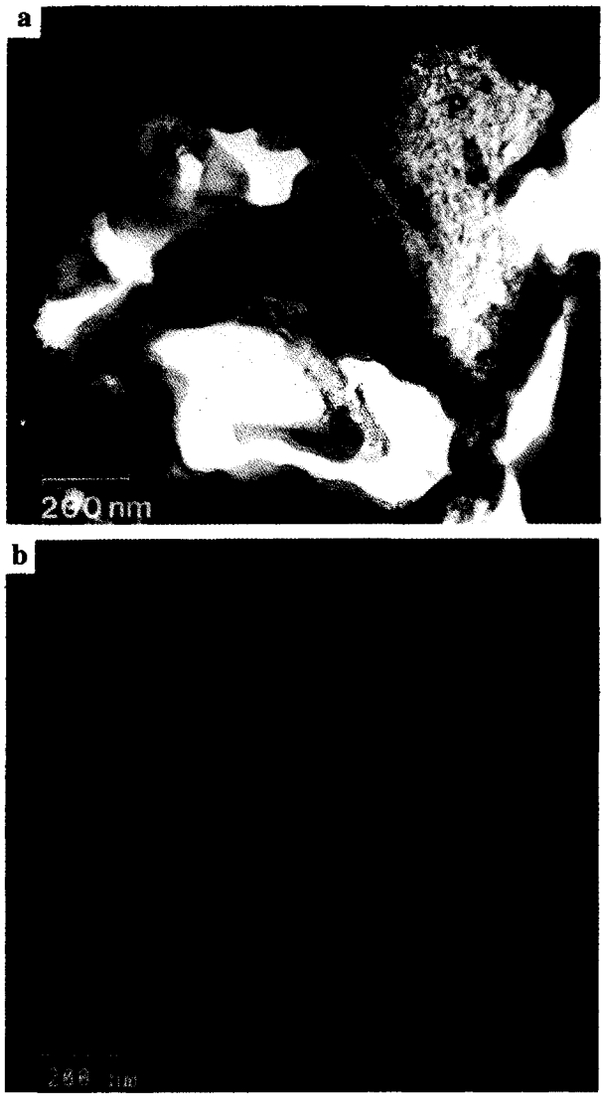

Fig. 5. (a) Microstructure of the material sintered at 1400°C. (b) The elemental distribution image shows that all the carbon (red) remains in pockets (denoted by P), while all the nitrogen (green and light blue) crystallises with an equivalent amount of Si and forms Si_3N_4 grains which are embedded in the glassy phase (dark blue).

from a large number of pockets (denoted by P in Fig. 5(a)) which show fine speckle contrast and have a diameter between 0·5 and 1 μm. Qualitatively, the chemistry of these two morphologically different parts of the microstructure could be clarified by ESI (Fig. 5(b)). The larger irregularly shaped grains all consist of Si_3N_4. The Si_3N_4 grains in the 1400°C material reach about half of the final grain size observed in the 1850°C composite.

Occasionally needle-like grains occur which contain both N and O and presumably consist of Si_2N_2O. They are also embedded within the glassy phase formed by the sintering additives. The pockets (P in Fig. 5(a)) are filled with a material showing speckle contrast and consisting mainly of Si and C. EDX and EELS analysis revealed that small amounts of Al, Y (less than 1 at%) and O

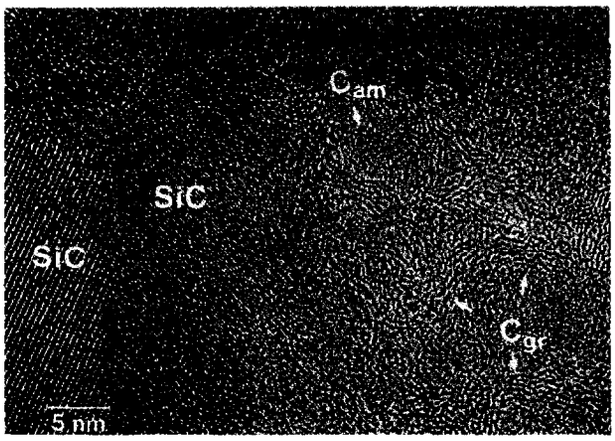

Fig. 6. High resolution image showing the atomic structure of the material contained within the pockets (P in Fig. 5). Nanocrystalline SiC can be identified by the corresponding lattice fringes. The SiC particles are embedded in graphitized and amorphous carbon.

(less than 5 at%) are also present. Electron diffraction patterns from these areas show Debye–Scherrer rings indicating that most of the material is nanocrystalline and that small SiC crystallites exist. In high resolution micrographs (Fig. 6) the SiC grains can be identified by their lattice fringes. Besides these, bent lattice fringes characteristic for graphitized carbon are also present. Both types of precipitate are embedded in amorphous carbon. The observed phase separation in the pockets is in agreement with the phase diagram of the binary Si–C system.[17]

Our microstructural results thus show that during the crystallisation at 1400°C a distinct phase separation takes place which leads to a demixing of the initial silicon-carbonitride into: (1) areas containing crystalline Si_3N_4 and Si_2N_2O grains which are embedded in the glassy phase formed by the sintering additives, and (2) pockets containing all the carbon in the form of nanocrystalline SiC and residual amorphous or graphitized carbon. It is important to note that, in the presence of the sintering additives, the initially amorphous silicon carbonitride has almost completely crystallised at 1400°C (even though the SiC is only nanocrystalline). In contrast to this, the monolithic silicon carbonitride (i.e. without sintering additives) remains amorphous at 1400°C even after 60 h of heat treatment. At 1400°C the sintering additives thus very effectively promote the crystallisation of the amorphous starting material. In the preparation of ceramic composites from polymer precursors the sintering additives are therefore not only required for densification but mainly to promote the crystallisation of the phases forming the composite.

The rapid onset of crystallisation at temperatures between 1300°C and 1400°C can be explained by the melting of the sintering additives.

The microstructure of the material at temperatures below 1300°C presumably consists of large amorphous silicon carbonitride particles which are mixed with crystalline Al_2O_3 and Y_2O_3 particles. In addition the SiNC particles are surrounded by an amorphous SiO_2 layer. In the system SiO_2 + Al_2O_3 + Y_2O_3 a deep eutectic exists at temperatures slightly above 1300°C. Between 1300 and 1400°C the sintering additives thus melt and the SiCN particles are embedded in a liquid phase. The crystallisation of the Si_3N_4 and Si_2N_2O phases is achieved by dissolution of Si and N in the liquid phase and reprecipitation of the crystalline phases. At a temperature of 1400°C only Si and N, but not carbon, diffuse out of the SiCN-particles and dissolve into the liquid phase which explains the observed phase separation into areas containing only Si_3N_4 and Si_2N_2O grains and remaining pockets consisting of nanocrystalline SiC and amorphous C. This result is also in agreement with the observation that sintering of SiC with Al_2O_3 and Y_2O_3 requires much higher temperatures before a solution–reprecipitation mechanism becomes operative.[5,6,8]

At temperatures above 1400°C further reactions are mainly expected in the pockets containing Si and C. At 1550°C grain coarsening occurs in the pockets and clusters of SiC grains form which are surrounded by pure carbon (Fig. 7). The existence of residual carbon can be explained by a surplus of carbon in the initial silicon carbonitride $Si_{3+x}N_4C_{x+y}$ with respect to the formation of stoichiometric Si_3N_4 and SiC. The transformation can be described by the reaction:

$$Si_{3+x}N_4C_{x+y} \xrightarrow{1400°C} Si_3N_4 + (x\ SiC_{nano} + y\ C)_p \xrightarrow{1550°C} Si_3N_4 + x\ SiC + y\ C^{(\uparrow)} \quad (1)$$

The first part of this reaction represents the initial silicon carbonitride, the second part the reaction product at 1400°C, in which the pockets P are filled with a mixture of nanocrystalline SiC and graphitized or amorphous C, and the third part the product at 1550°C, where the pockets are filled with precipitated SiC grains and amorphous carbon. At these temperatures the residual carbon obviously acts as a sintering aid for the SiC grains. At 1550°C the SiC does not seem to be wetted by the liquid phase formed by the sintering additives. Areas containing Si_3N_4 are still well separated from areas containing C and SiC. At 1550°C the residual carbon starts to disappear by forming gases. First indications for the onset of a reaction of the residual carbon with both the oxide phase and the Si_3N_4 grains are given by the gaps between the Si_3N_4 grains and the carbon rich areas. Three chemical reactions can be responsible for this:[18,19]

$$C + SiO_2 \rightarrow SiO\uparrow + CO\uparrow \quad (2)$$

$$3C + SiO_2 \rightarrow SiC + 2\ CO\uparrow \quad (3)$$

$$3C + Si_3N_4 \rightarrow 3SiC + 2\ N_2\uparrow \quad (4)$$

Reactions (2) and (3) lead to a decrease of the oxygen concentration of the material. Thermodynamically, the occurrence of reaction (4) is also expected.[19]

During sintering at 1700°C the amorphous carbon disappears completely. The SiC grains still occur mainly in clusters and the average grain size varies between 10 and 100 nm (Fig. 8). However,

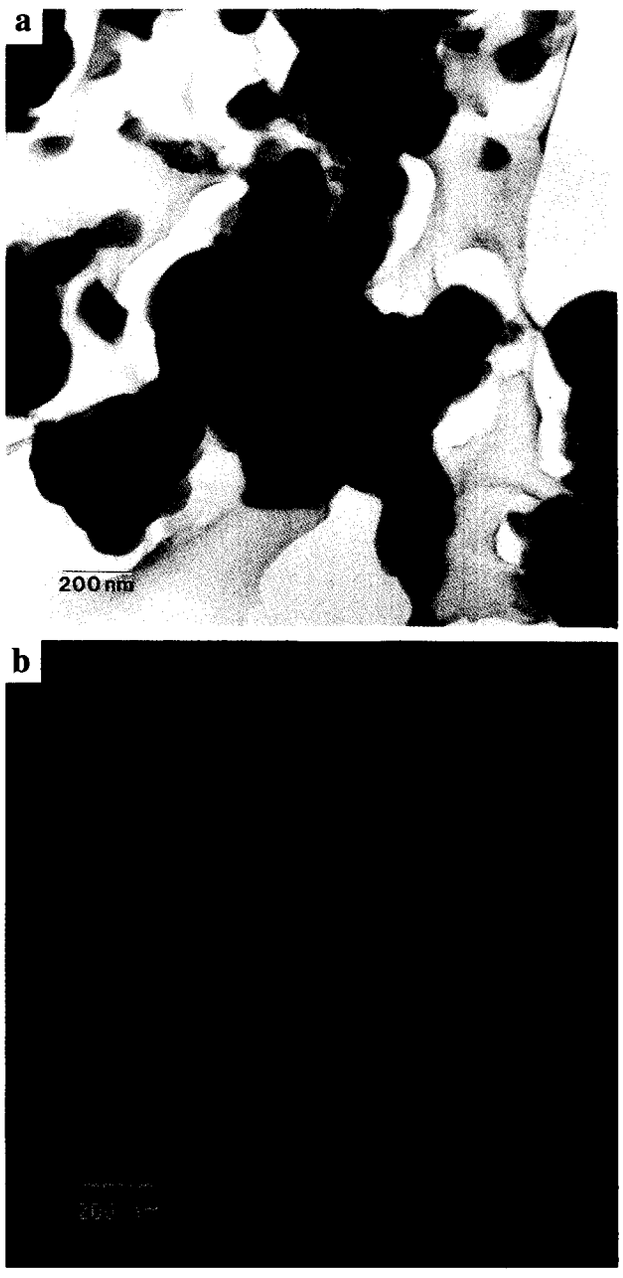

Fig. 7. Bright field (a) and elemental distribution image (b), carbon: red, nitrogen: green, and oxygen: blue) of the material sintered at 1550°C. Grain coarsening of the SiC within the residual C can be observed. At the same time, the residual carbon starts to react with the Si_3N_4 grains and the oxide phase which leaves gaps at the interfaces.

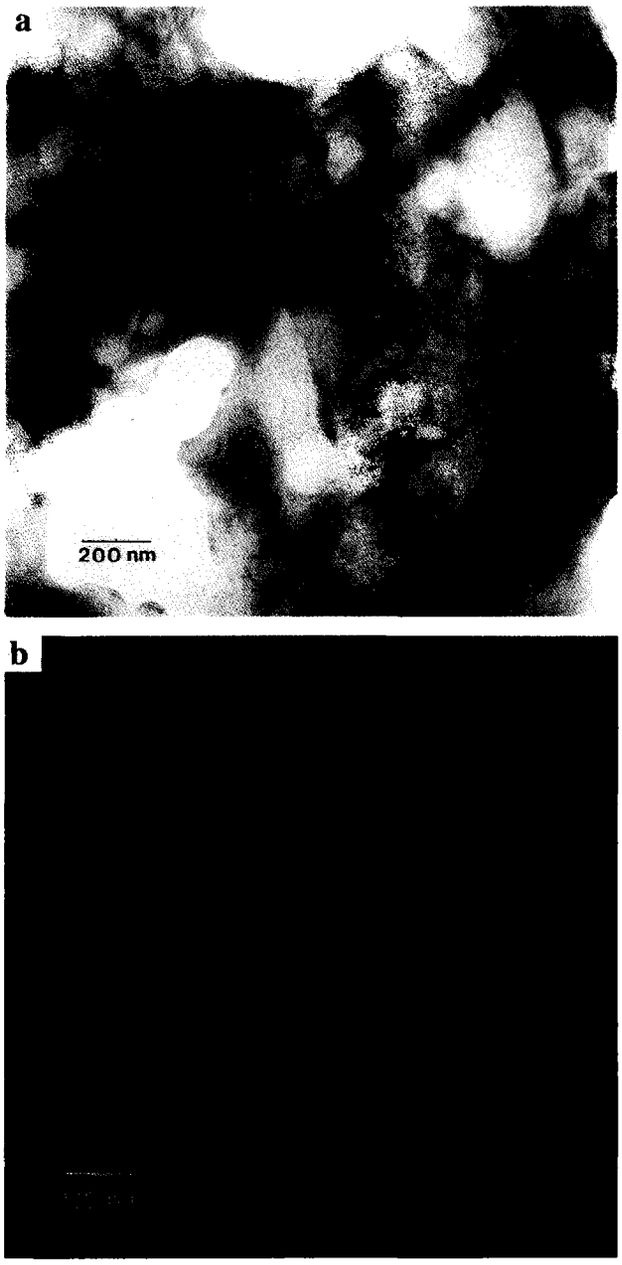

Fig. 8. Bright field (a) and elemental distribution image (b) carbon: red, nitrogen: green, and oxygen: blue) showing the microstructure of the material sintered at 1700°C. Clustering of the SiC particles (red) is still visible and most of the SiC particles have not reached the final grain size observed at 1850°C.

Fig. 8 shows that the SiC grains are now embedded within the glassy phase. From this we conclude that wetting of the SiC grains by the liquid oxides starts between 1550 and 1700°C. At 1700°C no more Si_2N_2O could be observed. This is in accordance with the thermal decomposition of the Si_2N_2O at temperatures above 1600°C:

$$3Si_2N_2O \rightarrow Si_3N_4 + 3SiO\uparrow + N_2\uparrow \qquad (5)$$

Between 1550 and 1700°C the reactions ((2)–(5)) lead to the production of gases which slow down densification.

After the disappearance of the amorphous carbon and the Si_2N_2O at 1700°C only the phases observed in the final product at 1850°C remain, i.e. SiC, Si_3N_4 and the oxidic glassy phase. An increase of the temperature to 1850°C thus only leads to gradual changes in the microstructure. These changes mainly are: a further grain growth of the SiC grains and a further densification. At 1850°C the grain growth of the SiC grains may also involve a solution/reprecipitation mechanism through the liquid phase. This results in an increasing intermixing of the SiC and Si_3N_4 grains leading to the final product described in 3.2.1.

3.2.3 Dependence on concentration of sintering additives

In the preceding section it has been shown that the sintering additives play an important role during the crystallisation of the amorphous silicon carbonitride. Therefore it can be expected that the concentration of the sintering additives also influences the resulting microstructure. In order to investigate this, composites were prepared with 5, 10 and 15% sintering additives under otherwise identical conditions (sintering for 1 h at 1850°C in 0·1 MPa N_2).

In the material with 5 wt% sintering additives, a large amount of open porosity is still present after sintering. This porosity can only be reduced by adding a larger amount of sintering additives, and at 15 wt% an almost completely dense material is obtained. These microstructural observations are in good agreement with the relative densities measured by porosimetry.[1]

In the samples sintered with 5 and 10 wt% sintering additives, a small number of Si_2N_2O grains are still present (Fig. 9). This observation is in contrast with the thermal decomposition of Si_2N_2O above 1600°C (Reaction (5)). However,

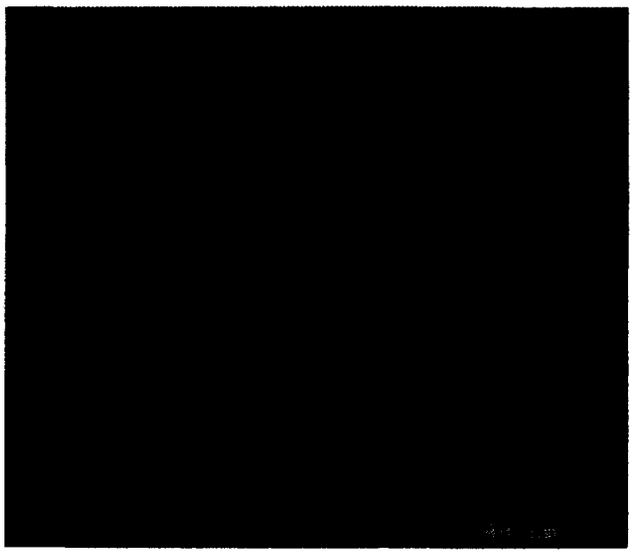

Fig. 9. In the samples sintered with 10 wt% sintering additives at 1850°C the microstructure consists of Si_3N_4 (green), SiC (red) and the amorphous oxide (blue). Occasionally Si_2N_2O grains could be observed, which in the ESI images are characterised by their mixed colour (here: mixed blue and green).

owing to the short annealing time of only 1 h, the Si_2N_2O grains may have survived for kinetic reasons and will disappear after longer heat treatments. The fact that Si_2N_2O is not found in the material sintered with 15% sintering additives indicates that the concentration of sintering additives and thus solution and reprecipitation processes play an important role in the thermal decomposition of Si_2N_2O.

From Fig. 9 it is also evident that the grain sizes of both SiC and Si_3N_4 are smaller in the material sintered with 5 or 10 wt% than in the reference material prepared with 15% additives. Hence, the rate at which the individual grains grow also shows a dependence on the concentration of the sintering additives. This can easily be understood for the Si_3N_4 while the fact that this grain size dependence is also observed for SiC indicates that solution/reprecipitation dominates the grain growth of SiC at 1850°C.

3.3 Sintered PCMSN-derived Si_2N_2O-ceramic

As discussed in Part I,[1] using ammonia during pyrolysis of the PCMSN results in the formation of amorphous silicon nitride powder. By attritor milling in wet isopropanol the reactive amorphous silicon nitride takes up oxygen in such an amount that during the subsequent sintering step polycrystalline Si_2N_2O can be produced. The sintering has to be performed at 1600°C because at higher temperatures Si_2N_2O decomposes according to Reaction (5). A mixture of Al_2O_3 and Y_2O_3 was used as sintering additives in concentrations of 3, 5,10 and 15 wt%.

In the TEM investigations submicron-size pores between the grains could be observed in the samples with 3 and 5% sintering additives. In these materials the low amount of sintering additives is not sufficient to close the pores during pressureless sintering. The individual Si_2N_2O grains are characterised by their elongated shape with an aspect ratio of 3–10 and by the high number of parallel stacking faults. In the materials with 3 and 5 wt% sintering additives only Si_2N_2O grains but no Si_3N_4 grains were found. In the ESI images the Si_2N_2O grains are characterised by their mixed colour (yellow) which is obtained by the superposition of the intensity which is present in both elemental distribution images (nitrogen: red and oxygen: green) (Fig. 10(a)). The oxidic glassy phase between the individual grains is characterised by the green colour.

At a concentration of 10 and 15 wt% of the sintering additives no more pores between the grains could be found. In the 10 wt% material occasionally Si_3N_4 grains could be observed and in the 15 wt% material the Si_3N_4 grains were present more frequently reaching concentrations of up to 10

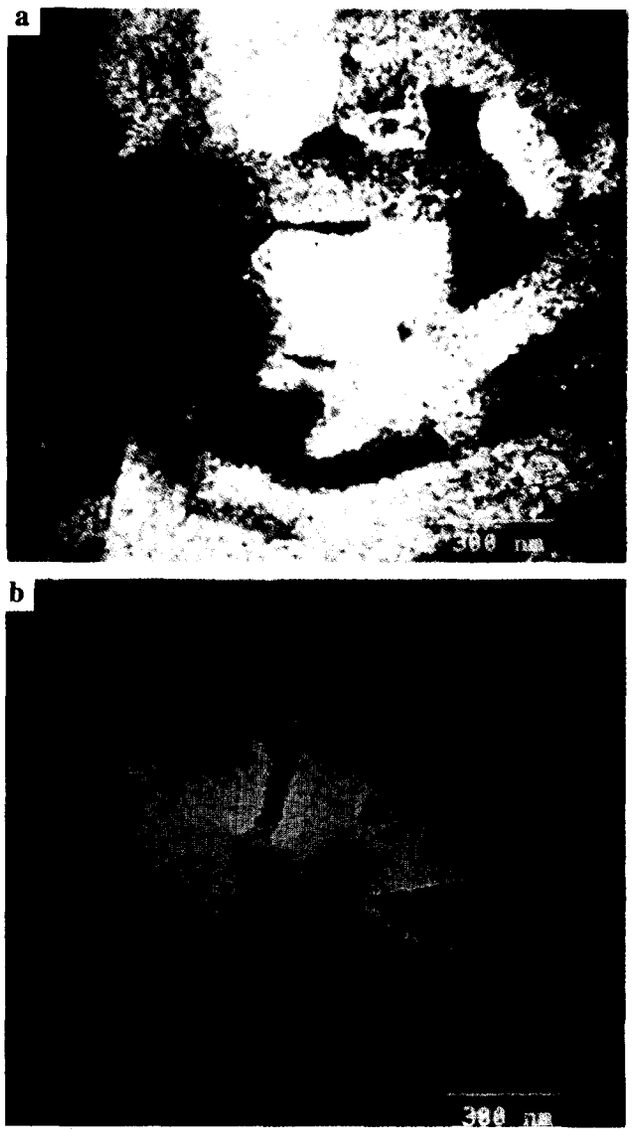

Fig. 10. The microstructure of the Si_2N_2O materials sintered with 3 wt% (a) and 15 wt% (b) sintering additives. In the images the nitrogen distribution is shown in red, the oxygen distribution in green. The Si_2N_2O grains are characterised by their mixed colour (red + green = yellow). At 3 wt% unfilled pores remain. In the 15 wt% samples the microstructure is dense but Si_3N_4 grains were present (red).

vol% (Fig. 10 b). The occurrence of Si_3N_4 grains is thus clearly dependent on the concentration of the sintering additives. This can be understood if it is assumed that during sintering the amorphous silicon nitride at least partly has to be dissolved in the liquid phase formed by the sintering additives. As discussed in the previous section the solution/reprecipitation mechanism may lead to a decomposition of Si_2N_2O into Si_3N_4, therefore increasing the amount of sintering additives increases the probability of Si_3N_4 precipitation.

3.4 Si_3N_4 sintered with 20 wt% Polysilane (PMPS)

According to the results described in Part I[1], an alternative way to produce Si_3N_4/SiC-composites is to mix Si_3N_4 powder with the polysilane PMPS

and an adequate amount of sintering additives. In our studies, 20 wt% of the PMPS and 12 wt% of sintering additives comprising 2·8 wt% AlN, 7·8 wt% Y_2O_3 and 1·4 wt% Al_2O_3 were used.

The resulting microstructure obtained after pyrolysis and sintering of the polymer-powder compact is shown in Fig. 11(a). Large grains with average grain sizes of 0·5–1 μm can be identified. Smaller particles with diameters of 20–200 nm surround these grains (intergranular) but are also embedded within the grains (intragranular). These particles are comprised of SiC as is clearly revealed by the ESI image (Fig. 11(b)). The larger grains consist of β-Si_3N_4. Therefore, besides the intergranular SiC, small intragranular SiC nanoprecipitates in the Si_3N_4 crystals could be detected in our material. A similar composite microstructure belonging to this mixed intra- and inter-type was first reported by Niihara *et al.*.[20] It was found that the fracture strength of these materials is considerably higher than the strength of Si_3N_4/SiC composites without intragranular SiC-precipitates.[9]

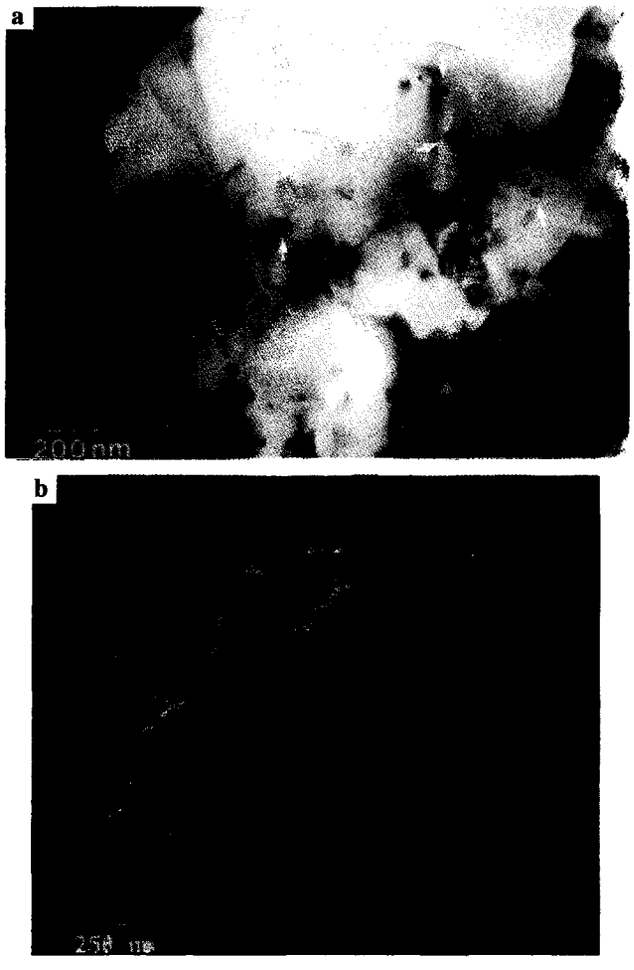

Fig. 11. Si_3N_4/SiC-composite material produced by sintering Si_3N_4 powder with 20 wt% of the PMPS precursor. In the bright field image (left) a number of precipitates can be observed in the large Si_3N_4 grains. The ESI image reveals that these precipitates consist of SiC nanoparticles (red). The Si_3N_4 grains are shown in green, the amorphous oxide in blue.

The results obtained on the Si_3N_4/SiC-composites produced from the polysilazane precursor (see Section 3.2.2) indicate that during sintering considerable amounts of the Si and N present in the starting material are dissolved in the liquid phase. In the material produced from the Si_3N_4-powder/polysilane mixture this solution–reprecipitation process will also take place leading to the growth of larger Si_3N_4 grains. During the reprecipitation of Si_3N_4 from the liquid phase, small polysilane derived SiC particles might become enclosed by the growing Si_3N_4 grains leading to the observed microstructure. The fact that this is not observed in the Si_3N_4/SiC-composites produced from polysilazane as described in Section 3.2.2 could be due to the observed phase separation into regions containing Si_3N_4 grains embedded in the glassy phase and regions containing SiC and residual C. Even though Si_3N_4 might dissolve and reprecipitate at higher temperatures, the SiC is well enough separated from the growing Si_3N_4 crystals and no enclosure is possible.

4 Conclusions

The processing of ceramic composites from polymer precursors involves a complicated sintering mechanism for which we have studied the dependence on the starting material and the processing conditions. The mechanism is based on the formation of a liquid phase from the sintering additives which, by surrounding the amorphous starting material, serves several purposes: (1) the onset of crystallisation occurs much faster and at lower temperatures; (2) the chemical reactions which lead to the formation of the stable, stoichiometric crystalline phases are accelerated by the diffusion through the liquid phase, and (3) complete densification of the material can only be achieved with sintering additives. Based on the results of our microstructural characterisation, a model of the processes occurring during sintering can be proposed (Fig. 12): β-Si_3N_4 grains and Si_2N_2O grains start to form by a solution–reprecipitation mechanism immediately after formation of the liquid phase (1400°C). An increase in temperature leads to grain coarsening by the same mechanism. SiC and C, at least at the lower temperatures, are not dissolved by the liquid phase and are left in pockets which are remnants of the initial SiCN particles. Nucleation and grain coarsening of the SiC grains at the lower temperatures only occurs within the residual carbon matrix. The phases formed are the thermodynamically stable phases β-Si_3N_4 and β-SiC. Chemical reactions at intermediate sintering temperatures result in the disappearance of the

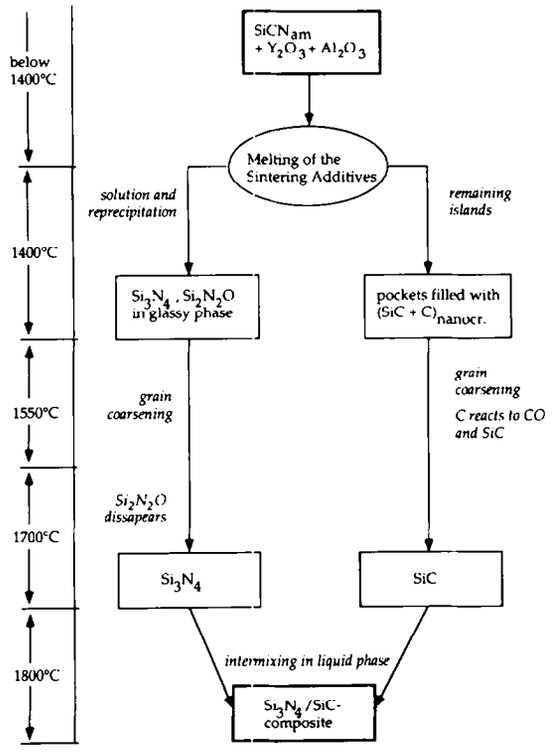

Fig. 12. Schematic diagram showing the processes occurring at increasing sintering temperatures in the Si_3N_4/SiC-composite material.

Si_2N_2O grains and the residual carbon. The gases produced during these reactions slow down densification. Further grain coarsening and rearrangements of the particles at the higher sintering temperatures lead to the final microstructure observed at 1850°C. In the final product the clustering of SiC grains is less pronounced than in the materials obtained at lower temperatures. We attribute this to a solution and reprecipitation reaction which at 1850°C also becomes operative for the SiC and leads to a redistribution of the SiC grains.

In our studies, elemental distribution images obtained with the ESI technique have proven to be a very efficient tool for the analytical characterisation of ceramic microstructures. A comparison with the phases identified by X-ray diffraction (see Part I of our studies[1]) confirms that our TEM results are representative for the overall micro-structure of the materials investigated. However, details of the microstructure, for example the inclusion of SiC precipitates in Si_3N_4 grains which is important for the mechanical behaviour of the resulting composite, could only be identified in the TEM studies.

Acknowledgement

The authors would like to acknowledge helpful discussions with R. Brook. The work was supported by: the Bundesministerium für Forschung und Technologie (NTS 0215/8), the European Community (BREU 0106-C-JR), the Keramikverbund Karlsruhe-Stuttgart, the KSB Foundation, Stuttgart, the Deutsche Forschungsgemeinschaft, and the Fonds der Chemischen Industrie, Frankfurt.

References

1. Riedel, R., Seher, M., Mayer, J. & Szabó, D. V., Polymer derived Si-based bulk ceramics, Part I: preparation, processing and properties. *J. Eur. Ceram. Soc.*, **15** (1995) 703.
2. Reimer, L., Fromm, I. & Rennekamp, R., Operation modes of electron spectroscopic imaging and energy-loss spectroscopy in a transmission electron microscope. *Ultramicroscopy*, **24** (1988) 339–54.
3. Hayashi, T., Munakata, H., Suzuki, H. & Saito, H. Pressureless Sintering of Si_3N_4 with Y_2O_3 and Al_2O_3. *J. Mat. Sci.*, **21** (1986) 3501–8.
4. Boberski, C., Bestgen, H. & Hamminger, R., Microstructural development during liquid-phase sintering of Si_3N_4 ceramics. *J. Eur. Ceram. Soc.*, **9** (1992) 95–9.
5. Omori, M. & Takei, M., Pressureless sintering of SiC. *J. Am. Ceram. Soc.*, **65** (1982) C-92
6. Kleebe, H.-J., SiC and Si_3N_4 materials with improved fracture resistance. *J. Eur. Ceram. Soc.*, **10** (1992) 151–9.
7. Lange, F. F., Effect of microstructure on the strength of the Si_3N_4/SiC composite system. *J. Am. Ceram. Soc.*, **56** (1973) 445.
8. Greil, P., Petzow, G. & Tanaka, H., Sintering and HIPping of silicon Nitride–Silicon carbide composite materials. *Ceramics Intern.*, **13** (1987) 19–25.
9. Sawaguchi, A., Toda, K. & Niihara, K., Mechanical and electrical properties of Silicon Nitride–Silicon Carbide nanocomposite material. *J. Am. Ceram. Soc.*, **74** (1991) 1142–4.
10. Sasaki, G., Nakase, H., Sukanuma, K., Fujita, T. & Niihara, K., Mechanical properties and microstructure of Si_3N_4 matrix composite with nano-meter scale SiC-particles. *J. Ceram. Soc. Japan*, **100** (1992) 536–40.
11. Rouxel, T., Wakai, F. & Izaki, K., Tensile ductility of superplastic Al_2O_3–Y_2O_3–Si_3N_4/SiC composites. *J. Am. Ceram. Soc.*, **75** (1992) 2363–72.
12. Lanio, S., High-resolution imaging magnetic energy filters with simple structure. *Optik*, **73** (1986) 99–107.
13. Krivanek, O. L., Gubbens, A. J., Dellby, N. & Meyer, C. E., Design and first applications of a post-column imaging filter. *Micros. Microanal., Microstruct.*, **3** (1992) 187–99.
14. Bihr, J., Benner, G., Krahl, D., Rilk, A. & Weimer, E., Design of an analytical TEM with integrated imaging Ω-spectrometer. *Proc. 49th Ann. Meeting EMSA*, ed. G. W. Bailey, San Francisco Press Inc., 1991, pp. 354–5.
15. Berger, A., Mayer, J. & Kohl, H., Detection limits in elemental distribution images produced by energy filtering TEM: case study of grain boundaries in Si_3N_4. *Ultramicroscopy*, **55** (1994) 101–12.
16. Salzberger, U., Strecker, A. & Mayer, J., TEM specimen preparation: A universal method for cross sections and brittle materials. *Electron Microscopy 92*, Vol. 2, eds A. Lopez-Galindo & M. J. Rodriguez-Garcia, Granada, Spain, 1992, pp. 743–4.
17. Fitzer, E., Hegen, D., *Angew. Chem.*, **91** (1979) 316.
18. Jong, B. W., Formation of silicon carbide from silica residues and carbon. *Am. Ceram. Soc. Bull.*, **58** (1979) 788.
19. Nickel, K. G., Hoffmann, M. J., Greil, P. & Petzow, G., Thermodynamic calculations for the formation of SiC whisker-reinforced Si_3N_4 ceramics. *Adv. Cer. Mat.*, **3**(6) (1988) 557.
20. Niihara, K., New design concept of structural ceramics — ceramic nanocomposites, *J. Ceram. Soc. Japan*, **99** (1991) 974–82.